Synthesis of a $NdAlO_3/Al_2O_3$ Ceramic−Ceramic Composite by Single-Source Precursor CVD†

Michael Veith,* Sanjay Mathur,* Nicolas Lecerf, Karsten Bartz, Manuela Heintz, and Volker Huch

Institute of Inorganic Chemistry, University of Saarland, D-66123 Saarbruecken, Germany

Received September 21, 1999
Revised Manuscript Received December 2, 1999

The incorporation of neodymium ions or nanoscaled Nd-based phases in insulating hosts has important applications as solid-state laser materials, phosphors for fluorescent lighting, optical amplifiers, etc.[1,2] A homogeneous distribution of Nd^{3+} ions, in a host matrix, is difficult to achieve due to their clustering tendency. To keep the Nd^{3+} ions homogeneously dispersed, alumina is added as a codopant which eliminates microscopic segregation by providing Nd^{3+} ions a favorable coordination state.[3] The Nd−Al oxide ceramics are usually prepared either from solid-state reaction of Nd_2O_3 and Al_2O_3[3] or by the CVD of $NdCl_3$ and $AlCl_3$.[4] Whereas the first method demands high temperatures (>1600 °C) for the diffusion of one component into the other, the limitations of the latter approach are the low vapor pressures of rare earth halides and the contamination of chloride ions, in the resulting ceramics. In this context, the use of a single-source metal−organic precursor containing preformed Nd−O−Al bonds can be a better route to nanophase Nd−Al oxide systems. Moreover, a multisource synthesis of Nd−Al−O ceramics using individual components is hampered by the lack of suitable Nd precursors with sufficient volatility. Besides an easy process control, the main advantages of the molecular precursor approach[5] are the atomic level mixing of the components, significantly low decomposition temperatures, and the absence of contaminating halide ions. We report here on the first deposition of thin films of nanoscaled $NdAlO_3/Al_2O_3$ composite by CVD.

The efficiency of CVD process depends crucially on the synthesis of high-purity precursors with a high vapor pressure and gas-phase stability.[5,6] The mixed-metal Nd−Al alkoxide, used in this study, was prepared following the procedure reported by Mehrotra.[7] Owing to a large number of conflicting reports[8] on the identity of lanthanide−aluminum mixed-metal alkoxides, we have performed a single-crystal diffraction analysis[9] to establish the structure and the heterometal composition of the precursor. The solid-state structure (Figure 1) of the molecule $[Nd\{Al(OPr^i)_4\}_3(Pr^iOH)]$ formally results from a bidentate ligation of three monoanionic tetraisopropoxo aluminate units ($\{Al(OPr^i)_4\}^-$) to a central Nd^{3+} cation. The strong chelation of $\{Al(OR)_4\}^-$ units (see Al−O bond distances, Figure 1) imparts a high stability to the heterometal framework resulting in an intact vapor transport of **1**. The molecule exists as an alcohol adduct, in the solid state; however, the "alcohol free" compound $[Nd\{Al(OPr^i)_4\}_3]$ is also thermally stable and could be obtained by the distillation of **1** under vacuum (110−115 °C/10^{-2} mbar).

The gas-phase pyrolysis of $[Nd\{Al(OPr^i)_4\}_3(Pr^iOH)]$ (**1**) was performed in a low-pressure chemical vapor deposition (LP CVD) apparatus. The experimental setup was similar to that described in the other studies from this group.[5c,d,10] The substrates (steel, copper, silicon) were heated inductively by a high-frequency generator. The precursor was directed to hot (500 °C) substrates at low pressures (10^{-2}−10^{-3} mbar) and the volatile byproducts formed in the thermolysis were on-line analyzed by a quadrupole mass spectrometer, coupled to the CVD assembly. The deposition of thin films was examined in the temperature range 400−550 °C. The growth rates were found to be significant (5−7 μm/h) at 500 °C and films of thickness 500 nm to 10 μm were deposited on different substrates, at this temperature. The films obtained at lower temperature (<500 °C) showed a high organic contamination (up to 4 at. %), whereas at higher deposition temperatures (above 550 °C), the adhesion of the films on the target substrate was poor and a significant amount of the product decomposed in the gas phase before reaching the target. The films obtained were purple colored with a glassy appearance. The SEM images (Figure 2) revealed smooth surfaces made up of spherical particles which was complemented by AFM studies (see later). The mass spectra revealed isopropyl alcohol, acetone, propene, and hydrogen as the pyrolysis products; the decomposition mechanism (ionic and/or

† Dedicated to Professor Arndt Simon on the occasion of his 60th birthday.

* Corresponding authors: Prof. Michael Veith/Dr. Sanjay Mathur, Institute of Inorganic Chemistry (Geb. 23.1), University of Saarland, D-66123 SAARBRUECKEN, Germany. E-mail: veith@rz.uni-sb.de and mathur@ch11sgi0.anchem.uni-sb.de.

(1) Blasse, G. *Chem. Mater.* **1989**, *1*, 294.
(2) Tissue, B. M. *Chem. Mater.* **1998**, *10*, 2837.
(3) Ikesue, A.; Kinoshita, T.; Kamata, K.; Yoshida, K. *J. Am. Ceram. Soc.* **1995**, *78*, 1033.
(4) Arai, K.; Namikawa, H.; Kumata, K.; Honda, T.; Ishii, Y.; Handa, T. *J. Appl. Phys.* **1986**, *59* (10), 3430.
(5) (a) Veith, M.; Altherr, A.; Lecerf, N.; Mathur, S.; Valtchev, K.; Fritscher, E. *Nanostruct. Mater.* **1999**, *12*, 191. (b) Meyer, F.; Hempelmann, R.; Mathur, S.; Veith, M. *J. Mater. Chem.* **1999**, *9*, 1755. (c) Veith, M.; Faber, S.; Hempelman, R.; Janssen, S.; Prewo, J.; Eckerlebe, H. *J. Mater. Sci.* **1996**, *31*, 2009. (d) Veith, M.; Mathur, S.; Lecerf, N.; Hao, S.; Huefner, S. *Chem. Mater.* **1999**, *11*, 3103.
(6) (a) Belot, J. A.; Wang, A.; McNeely, R. J.; Liable-Sands, L.; Rheingold, A. L.; Marks, T. J. *Chem. Vap. Deposition* **1999**, *5*, 65. (b) Jones, A. C. *Chem. Vap. Deposition* **1999**, *4*, 169. (c) Puddephatt, R. J.; Pollard, K. D. *Chem. Mater.* **1999**, *11*, 1069. (d) Wernberg, A. A.; Gysling, H. J. *Chem. Mater.* **1993**, *5*, 1056. (e) Rocheleau, R. E.; Zhang, Z.; Gilje, J. W.; Meese-Marktscheffel, J. A. *Chem. Mater.* **1994**, *6*, 1615.
(7) Mehrotra, R. C.; Mehrotra, A. *Indian J. Chem.* **1972**, *10*, 532.
(8) (a) Poncelet, O.; Sartain, W. J.; Hubert-Pfalzgraf, L. G.; Folting, K.; Caulton, K. G. *Inorg. Chem.* **1989**, *28*, 263. (b) Mehrotra, R. C.; Singh, A.; Tripathi, U. M. *Chem. Rev.* **1991**, *91*, 1287.
(9) Crystal data for $[Nd\{Al(OPr^i)_4\}_3 \cdot Pr^iOH]$: triclinic, space group, $P\bar{1}$, $a = 12.932(3)$ Å, $b = 13.779(3)$ Å, $c = 18.580(4)$ Å, $\alpha = 75.51(3)°$, $\beta = 85.76(3)°$, $\gamma = 62.82(3)°$, $V = 2848.4(11)$ Å^3, $Z = 2$. Diffraction data were collected on a Stoe AED 2 diffractometer operating with graphite-monochromated Mo Kα X-ray radiation ($\lambda = 0.71073$ Å). The structure was solved using direct methods (SHELXS-86) which revealed most of the heavy atoms from the electron density maps. The remaining non-hydrogen atoms were located from successive difference Fourier map calculations. The refinements were carried out using full-matrix least-squares techniques (SHELXL-97). Positions of non-hydrogen atoms were refined anisotropically. The hydrogen atoms were added as idealized contributions. Final R indices [$I > 2\sigma(I)$]: $R_1 = 0.0489$, $wR_2 = 0.1271$. R indices (all data): $R_1 = 0.0558$, $wR_2 = 0.1347$.

10.1021/cm991149g CCC: $19.00
Published on Web 02/02/2000

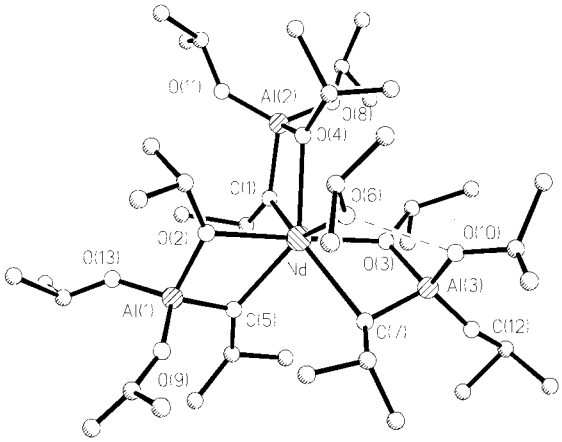

Figure 1. Molecular structure of $[Nd\{Al(OPr^i)_4\}_3(Pr^iOH)]$. Selected bond distances (Å) and angles (deg): Nd(1)−O(2), 2.385(4); Nd(1)−O(3), 2.400(4); Nd(1)−O(1), 2.404(4); Nd(1)−O(4), 2.427(4); Nd(1)−O(5), 2.429(4); Nd(1)−O(7), 2.495(4); Nd(1)−O(6), 2.553(5); av Al−O (terminal), 1.690; av Al−O (bridging), 1.788 [the dotted line indicates the interaction between the hydroxy proton of the coordinated alcohol ligand (O(6)) and the oxygen atom of the terminal $-OPr^i$ ligand (O(10)) present on Al(3)]; O(6)−O(10), 2.819; O(1)−Nd(1)−O(4), 62.29(13); O(3)−Nd(1)−O(7), 61.98(15); O(2)−Nd(1)−O(5), 121.31(14); O(4)−Nd(1)−O(6), 79.84(15); O(2)−Nd(1)−O(1), 94.76(15); O(7)−Nd(1)−O(6), 70.86(15); O(2)−Nd(1)−O(3), 174.85(13); O(2)−Nd(1)−O(3), 174.85(13); O(5)−Nd(1)−O(6), 127.07(15); O(1)−Nd(1)−O(6), 141.99(15); O(2)−Nd(1)−O(4), 88.95(13); O(4)−Nd(1)−O(7), 138.40(14); O(3)−Nd(1)−O(1), 88.14(15); O(1)−Nd(1)−O(7), 137.39(14).

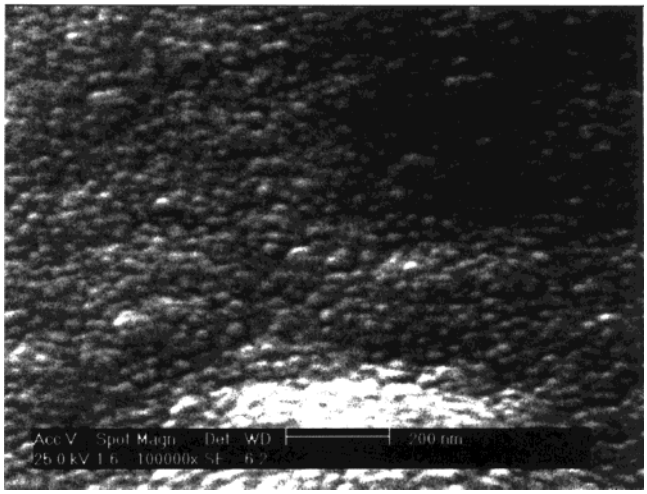

Figure 2. Scanning electron micrograph of the film deposited at 500 °C on a steel target.

radical) of the $-OPr^i$ ligand is not being discussed here. The identification of the gaseous products was achieved by recording the mass spectrum of the individual components under similar experimental conditions. A differential peak analysis performed by stripping sequentially the observed fragmentation patterns, of the standard samples, from the complete mass spectra recorded during the CVD process conformed to the decomposition reaction:

$$[Nd\{Al(OPr^i)_4\}_3(HOPr^i)] \xrightarrow{\text{CVD, 500 °C}} NdAlO_3/Al_2O_3 + (x+1)Pr^iOH + yCH_2{=}CH{-}CH_3 + z(CH_3)_2C{=}O + mH_2 \quad (1)$$

where $x/y \neq 1$, $x \gg y$, z, m and $x + y + z = 12$).

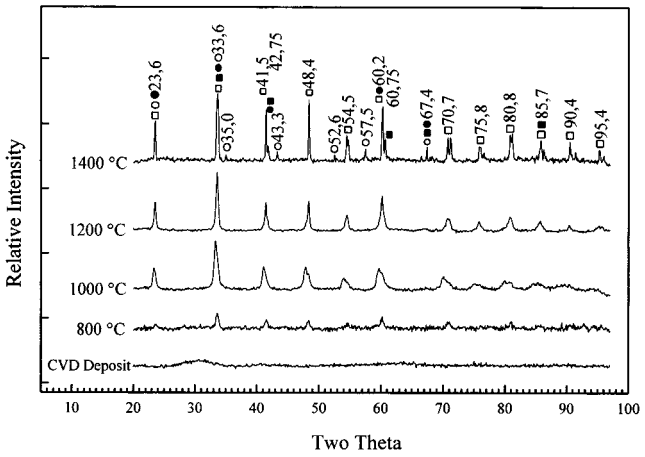

Figure 3. Room-temperature XRD powder trace of the film material sintered at different temperatures: (□) PDF [29-56] $NdAlO_3$ phase; (■) PDF [10 425] γ-Al_2O_3 phase; (●) PDF [04-877] δ-Al_2O_3 phase; (○) PDF [04-878] κ-Al_2O_3 phase.

The average metal ratios determined by energy-dispersive X-ray analysis in as-obtained and annealed samples correspond (±1.5%) to the metal stoichiometry (Nd:Al = 1:3) present in the precursor and in both the cases no element segregation was observed on a submicrometer level. The quantification of the results was achieved by measuring standards and employing the SEM Quant software with a ZAF correction procedure which revealed the formal composition to be $NdAl_3O_6$. The determination of Nd and Al contents by chemical analysis of the solid deposits corroborated the EDX analysis. The upper limit of embedded carbon impurities introduced during the CVD process was ∼2 at. %. The carbon content in the heat treated (800 °C) films was significantly low (<0.3%).

The films obtained after the CVD (500 °C) were strongly attached to the substrates; however, solid product could be obtained on quenching the hot substrates with a cold helium stream. The flakes of pure deposits were grained and filled in glass capillaries for X-ray diffraction studies. The deposits obtained at 500 °C are amorphous (XRD, Figure 3) and postannealing was necessary for the identification of crystalline phases. The XRD pattern of the CVD deposit sintered at 800 °C shows $NdAlO_3$ (JCPDS card no. [29-56])[11] to be the only crystalline phase (Figure 3). The diffraction peaks were broad, probably due to an incomplete crystallization process or very small crystallite size. Together with the formal chemical composition ($NdAl_3O_6$) of films and the broad XRD features at lower 2θ values (typically observed in aluminates[12,13] with a high amorphous content) indicates alumina to be the second phase. Curiously, the alumina, in the obtained composite, remained amorphous until 1200 °C which is higher than the temperature normally required for the crystallization of γ-alumina (∼750 °C).[13] Nevertheless, the crystallization of transition aluminas (mixture of γ, κ, and δ phases, JCPDS card nos. [10-425], [04-878], and [04-

(10) Veith, M.; Kneip, S. *J. Mater. Sci. Lett.* **1994**, *13*, 335.
(11) JCPDS Powder Diffraction File. Joint Committee for Powder Diffraction Standards, 1990; file card nos. [29-56], [10-425], [04-878], and [04-877].
(12) Veith, M.; Altherr, A.; Wolfanger, H. *Adv. Mater.* **1999**, *5*, 87.
(13) Urretavizacya, G.; Cavalieri, A. L.; Porto Lopez, J. M.; Sobrados, I.; Sanz, J. *J. Mater. Synth. Process.* **1998**, *6*, 1.

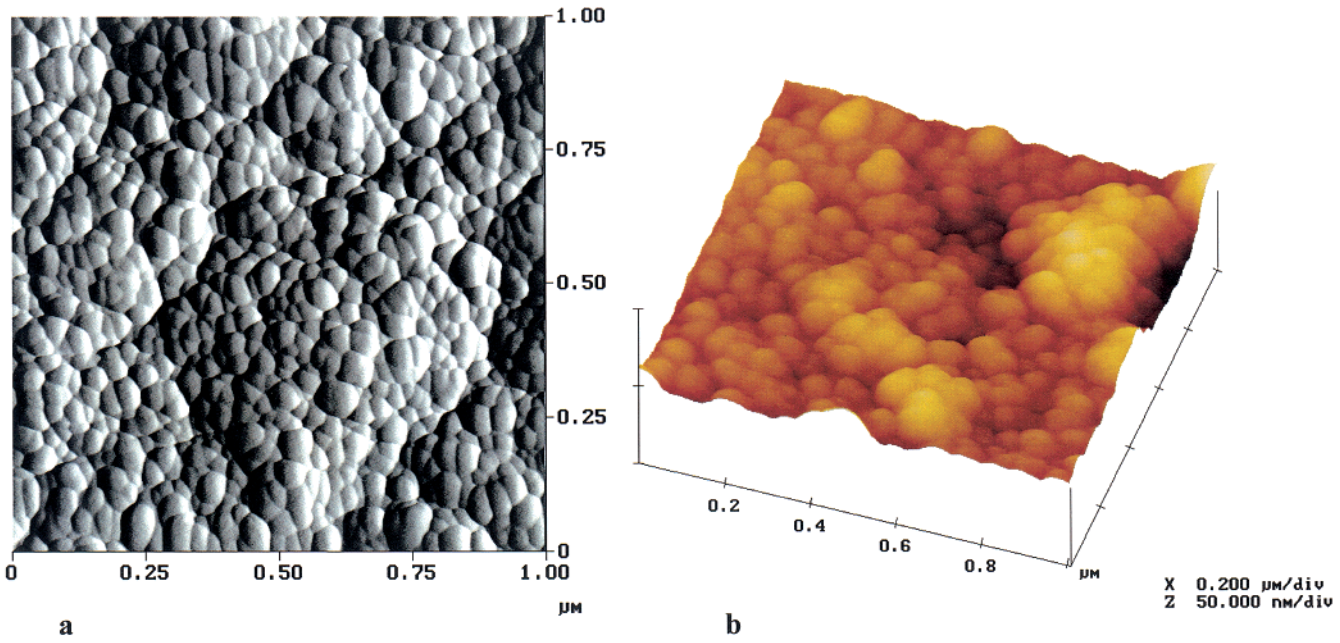

Figure 4. AFM images of the film obtained at 500 °C on a silicon wafer: (a) topographic (100 × 100 nm^2) and (b) 3D representation.

877], respectively)[11] was observed at 1400 °C (Figure 2). The slow crystallization of alumina and the steady growth of the $NdAlO_3$ crystallites illustrates how the coexistence of one phase can influence the crystallization behavior of the other in nanocomposites formed by a single precursor.

The films are nonconducting and since their roughness lies in nanometer scale, the surface morphology and microstructure of the films were examined by atomic force microscopy, using silicon or silicon nitride tips, on a Nanoscope III microscope of Digital Instruments. The AFM images, in friction (contact mode) and 3D (tapping mode) modes of a film deposited (500 °C) on a silicon target, are shown in Figure 4a and b, respectively. The friction image shows an even globular topology with particles of an average diameter of 30−40 nm while the 3D image exhibits the elevation (roughness) ranging from 20 to 50 nm.

The depth-resolved compositional homogeneity, with respect to the elemental distribution in the films, was obtained by glow discharge mass spectromeric analysis (GDMS) on a GLOQUAD spectrometer (VG Elemental) working with a low-pressure argon plasma. A typical GDMS depth profile obtained for Nd−Al−O system is shown in Figure 5. The graph shows the data after applying RSF (relative sensitivity factor) correction which is related to the emission intensity of a specific element.[14] The RSF values were determined by analyzing standard mixtures of pure aluminum and neodymium oxides in 3:1 molar ratio with known sputtering rates. The RSF corrected depth profile (Figure 5) shows three distinct regions: (i) the first minor part (scans 0−10) corresponds to adsorbants film (surfacial contamination); (ii) the second and the major part (scans 10−75) represents the film material and reveals the consistency level of element ratios in the solid film; (iii) the coating−substrate interface shows up in the third part as indicated by a reduced level of signal corresponding to the film compostion and the dominance of the substrate material (Fe) at higher scan numbers (scans above 75). The results illustrate that the Nd:Al ratio in the films corresponds to that present in the molecular precursor (Nd:Al = 1:3). The molar ratio of expected elements (Nd, Al, and O) obtained by plotting the element ratios against the number of scans gave the O:Al ratio of 2:1 which corresponds to the expected value in $NdAl_3O_6$. These observations confirm the CVD deposits to be pure oxidic films of formal composition $NdAl_3O_6$, a fact also borne out by the EDX and elemental analyses.

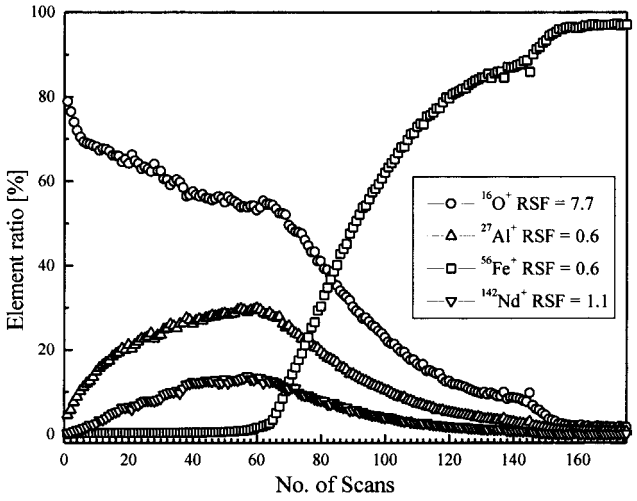

Figure 5. GDMS profile of a Nd−Al−O film deposited on steel, after applying the RSF correction.

In the TEM studies, the film material sintered below 800 °C, shows a homogeneous distribution of particles with nearly equal sizes; however, they differed in the morphology and composition. The EDX analysis revealed the composition to be $NdAlO_3$ and Al_2O_3 while the selective-area electron diffraction (SAED) pattern exhibited a high amount of diffuse scattering, indicating the ceramic to be largely amorphous. The alumina content remained X-ray amorphous until 1200 °C; how-

(14) Harrison, W. W.; Hess, K. R.; Marcus, R. K.; King, F. L. *Anal. Chem.* **1986**, *58* (2), 3411.

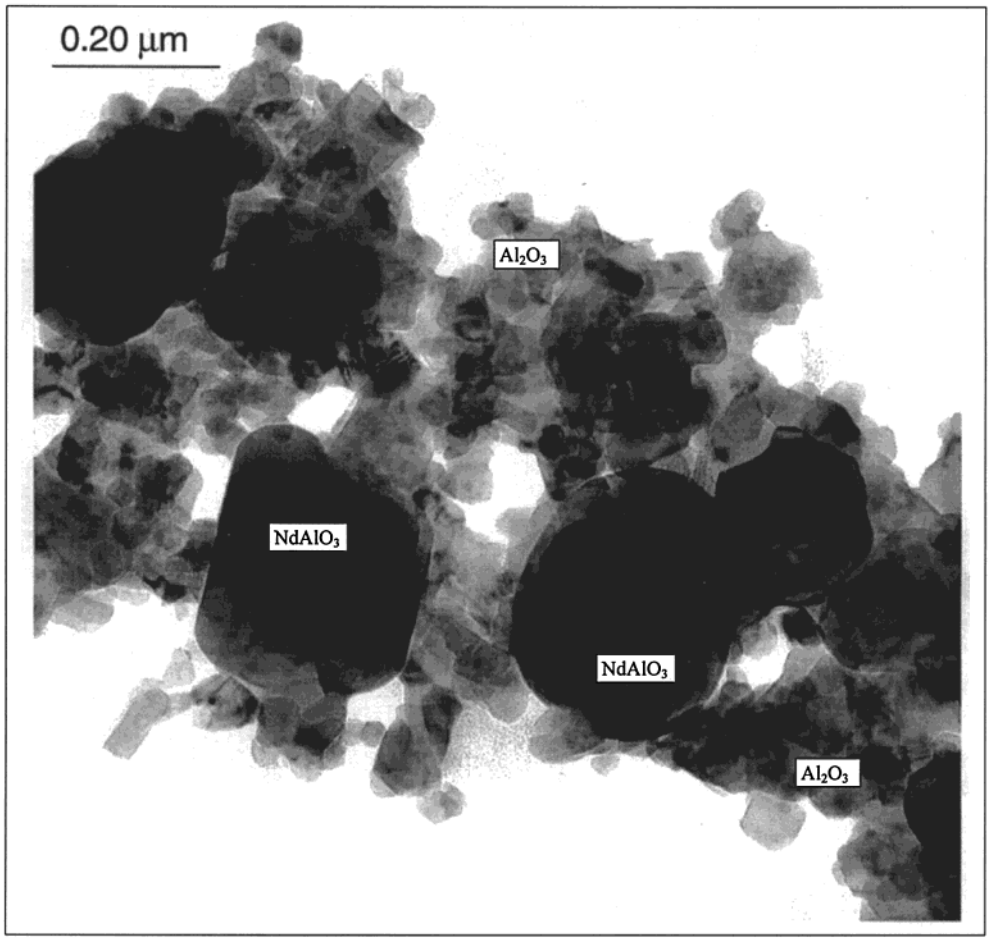

Figure 6. TEM image of the CVD deposit after sintering at 1400 °C.

ever, well-faceted grains with Al_2O_3 composition (EDX) were observed in the TEM images of powders sintered at 1000 °C. The sintering at higher temperature (1400 °C) gave a bimodal grain size distribution (Figure 6) of two nanocrystalline phases as confirmed by the XRD measurements. The characteristic grain sizes are 20−40 (Al_2O_3) and 200−300 ($NdAlO_3$) nm. The composition of larger grains, determined by spot EDX analysis, corresponds to $NdAlO_3$ whereas the smaller particles forming the matrix are of alumina. In summary, the present work demonstrates the use of heterometal alkoxides, generally used for producing high-homogeneity in the single-phase ceramics, to obtain a ceramic−ceramic composite of two distinct nanocrystalline phases (nanoheterogeneity).

Acknowledgment. The authors gratefully acknowledge the Deutsche Forschungsgemeinschaft for the financial support in the framework of the research program Sonderforschungsbereich 277 at the University of Saarland, Saarbruecken. The Alexander von Humboldt Foundation, Germany, is gratefully acknowledged for a research fellowship to S.M.

Supporting Information Available: Scanning electron micrographs of the as-deposited films (two images) [also available from one of the authors (S.M.)] and crystallographic data of **1**. This material is available free of charge via the Internet at http://pubs.acs.org.

CM991149G